International journal of basic and applied research

www.pragatipublication.com

ISSN 2249-3352 (P) 2278-0505 (E)

Cosmos Impact Factor-5.86

AN ADVANCED CONTROL STRATEGY FOR A HYBRID MICROGRID POWERED BY A DIESEL GENERATOR, PHOTOVOLTAIC (PV) SYSTEM, AND WIND TURBINE

[1]MR. G. GNANESHWAR KUMAR, [2]SRAVANI VADLA, [3]P.VAMSHI KRISHNA, [4]S.ASHISH

[1](Assistant professor), EEE. Guru Nanak Institutions Technical Campus, Hyderabad.

[234]B.Tech Scholars, EEE. Guru Nanak Institutions Technical Campus, Hyderabad.

Abstract— This study offers a green energy alternative for a microgrid for a location that relies on a diesel generator (DG) to supply all of its electrical needs. This microgrid is fueled by two renewable energy sources: a solar photovoltaic (PV) array and wind energy utilising a doubly fed induction generator (DFIG). The back-to-back voltage source converters (VSCs) attached in the rotor side of the DFIG have a shared DC bus that is directly connected to the solar PV array. Moreover, a bidirectional buck/boost DC-DC converter is attached to the same DC bus as a battery energy storage (BES) to offer a path for any extra DFIG stator power. With the regulation of the bidirectional buck/boost DC-DC converter and the rotor side VSC, respectively, the maximum power from both wind and solar is extracted. To get the most power out of a solar PV array, a modified perturb and observe (P&O) technique is described. Moreover, the control of load side VSC is made to optimise DG fuel usage. The reference DG power output for ideal fuel usage is determined using a new generalised approach. Using the SimPowerSystems tool box of MATLAB, the microgrid is modelled and simulated for a variety of scenarios, including changing wind speeds, changing insolation, the impact of changing load conditions on a bidirectional converter, and an unbalanced nonlinear load connected at the point of common coupling (PCC). The DG currents and DFIG stator currents are found to be sinusoidal and balanced.

Index Terms: Battery energy storage, doubly fed induction generator (DFIG), diesel generator, solar photovoltaic array, bidirectional buck/boost DC-DC converter.

1.INTRODUCTION

For the following reasons [1]–[3], diesel generators (DGs) are widely used in urban housing societies for both decentralised power generation and backup power.

• DGs are dispatchable and portable.

• Their capital costs are lower.

In comparison to other energy sources, DGs have higher conversion efficiency, which results in lower particular greenhouse gas emissions and easier maintenance.

They are frequently utilised for the power distribution of islands, commercial and military ships, etc. for the aforementioned reasons [4]. However, DGs experience increased operating costs, noise, and air pollution. The amount of fuel consumed based on the power generation determines the running cost. By putting in renewable energy (RE) sources like wind, solar, and biomass, among others, this expense is kept to a minimum. Moreover, RE-based power sources are abundant and pollution-free in nature. Because to their lower cost and developments in technology, wind and solar energy are thought to be more popular among RE sources. [5], [6]. The two primary types of wind turbines are fixed speed and variable speed. Due to their straightforward operating qualities, fixed speed wind turbines have been utilised in the past. They experience greater power loss, though. Due to their advantages, such as a decreased converter rating, less acoustic noise, excellent energy efficiency, and low power loss, variable speed wind turbines with doubly fed induction generators (DFIG) are the most widely utilised for wind energy extraction [7]. There is a wealth of information on DFIG-based wind energy conversion systems (WECS), both in grid-connected and standalone modes [9]–[11]. In [8], the authors describe a standalone DFIG-based WECS that uses a battery energy storage system (BES) that is directly connected to the DC link. Furthermore mentioned is the performance comparison between BES and no BES. For efficient operation of wind turbines combined with DFIG both in balanced and unbalanced grid settings, the authors of [9] have presented an expanded active power theory. Also, the rotor side converter is the only device used to regulate the DFIG (RSC). As a result, the topology experiences power quality problems, particularly under harmonic loads. The effect of phase locked loop parameters and grid strength on the stability of the DFIG wind farm in grid connected mode has been studied by Liu et al. [10]. Yet no experimental validation has been carried out. The authors of [11] have covered a synchronisation control mechanism for DFIG's seamless connection to the grid. Additionally, it has been put into practise utilising a real-time simulation platform using a modified IEEE 39 bus system. Hardware realisation, however, has not been completed. On the other hand, solar photovoltaic (PV) array electricity generation has increased globally. Single stage or two stage solar energy conversion systems (SECS) are both possible. [12] and [13] report on some of the solar PV system literature. The single stage SECS connected to the electric grid has been shown by Shah et al. [12]. Also, a fundamental current extraction method for voltage source converters based on a second-order generalised integrator with a frequency locked loop has been implemented (VSC). The authors of [13] have shown the grid-interacting double stage SECS. To address the power quality difficulties, VSC has also adopted an adaptive fast zero attracting normalised least mean fourth algorithm. Due to their sporadic nature, the operation of WECS and SECS independently is neither affordable nor dependable. As a result, the reliability of power generation is increased by the combination of both wind and solar sources [14], [15]. The wind-PV system by Morshed et al. [14] has the ability to ride around faults. In its topology, a boost converter and a DC-DC converter are used to connect the solar PV array to the DC connection of the DFIG-based WECS. Due to the additional grid side converter and DC-DC converter, switching costs and losses are, however, increased. The wind-solar PV system with BES has been shown by the authors in standalone mode in [15]. In its current arrangement, a boost converter connects the solar PV array to the DC link of the wind turbine-driven DFIG. Unfortunately, because BES is directly connected to the DC link, the current flowing through it cannot be controlled. Also created and published in the literature are microgrids based on DG, wind, and solar sources [16]–[18]. The capacity planning of BES for an island-based microgrid powered by wind, solar, and diesel sources is covered by the authors in [16]. Unfortunately, there hasn't been any discussion about DG's ideal fuel operation. For a fuel-efficient zone with BES, the authors of [17] have developed a wind-diesel microgrid. Yet, because of its direct connection at the DC link, the BES current is not controlled. Also, connecting only one RE source increases the likelihood of leaving the fuel-efficient zone. A wind-solar-diesel microgrid using BES has been presented by Venkatraman et al. [18] for a specific isolated location. Nevertheless, when the source and load controllers were being developed, the ideal DG operation was disregarded. The BES is essential in any microgrid when there is a mismatch between demand and generation. Also, it aids in maximising power output from solar and wind sources, particularly when production exceeds demand. In order to extract the maximum power corresponding to a specific wind speed and insolation, respectively, there are numerous maximum power point tracking (MPPT) algorithms addressed in the literature [12], [13], [15], [19], [20].

International journal of basic and applied research

www.pragatipublication.com

ISSN 2249-3352 (P) 2278-0505 (E)

Cosmos Impact Factor-5.86

In order to reduce DG fuel consumption, this work provides a microgrid that consists of DFIG, DG, and solar PV arrays with BES that are driven by wind turbines. In this case, the DG is made to provide the necessary base load for a specific neighbourhood of houses. The following are the primary contributions of this work to the control components of the scheme.

• In order for the DG to continue running in the best fuel consumption mode, the reference DG power output is computed using a novel generalised idea.

• The load side converter control (LSC) is intended to control reactive power compensation, load imbalance compensation, and harmonics compensation in addition to DG.

• The RSC control is made to get the most power possible out of the wind turbine.

A bidirectional buck/boost DCDC converter connects the BES to the shared DC bus of back-to-back coupled VSCs. It intends to offer a conduit for DFIG's extra stator power. A solar PV array is additionally directly connected to a DC bus.

• In order to get the most power out of the solar PV array and to manage the current through BES, the bidirectional buck/boost DC-DC converter control was created.

• To maximise power from a solar PV array, a modified perturb and observe (P&O) MPPT algorithm is described.

• This microgrid layout uses the fewest possible converters, which lowers the overall system cost and switching losses.

• The DFIG stator currents and DG currents are kept sinusoidal and balanced in accordance with IEEE 519.

The SimPowerSystems tool box of MATLAB is used to model and simulate the wind-diesel-solar microgrid with BES. Variable wind speeds, fluctuating insolation, the impact on the buck boost converter at various loads, and an unbalanced nonlinear load linked at the point of common coupling are all taken into account when analysing the system performance (PCC).

2. CONFIGURATION OF MICROGRID

Figure 1 shows the microgrid's schematic configuration. Wind turbine, DFIG, DG, solar PV array, BES, bidirectional buck/boost DC-DC converter, RSC, LSC, interfacing inductors, Y/Y transformer, linear and nonlinear loads, circuit breakers (CB1 & CB2), DC link capacitor, ripple filters, etc. are all included in it. This microgrid is intended to provide 7.5 kW of peak power for a specific location. The solar PV array and wind turbine generator are each intended to produce 7.5 kW of power. In this configuration, the BES is connected via a bidirectional buck/boost DC-DC converter, while the solar PV array is connected directly to the DC link. The DG consists of a 4 pole synchronous generator, a 4 stroke reciprocating internal combustion engine, and an automatic voltage regulator (AVR). In accordance with the wind turbine generator's rated capacity, a 7.5 kVA DG is chosen. Based on the literature mentioned in [12], [15], and [17], the design of a wind turbine generator, solar PV array, DG, BES, and other components is carried out. Additionally, the Appendices provide information on the microgrid design parameters.

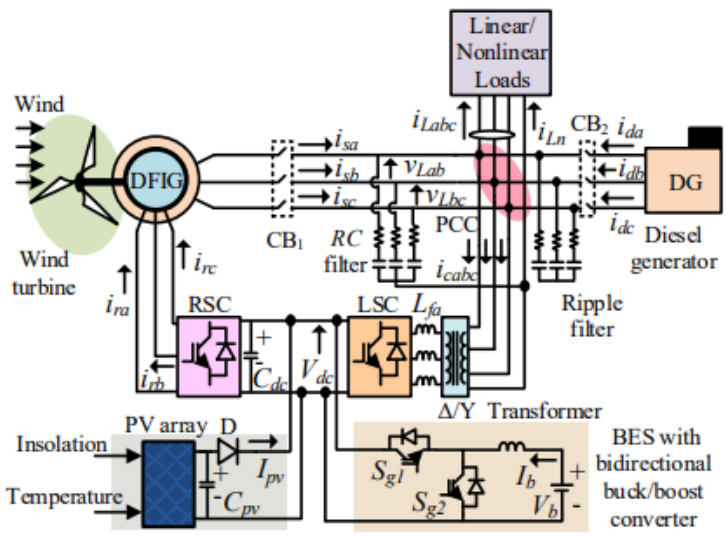

Fig 2.1 DFIG based microgrid.

3. CONTROL ALGORITHMS OF MICROGRID

The complete description of control algorithms of RSC and LSC, MPPT algorithm of solar PV array, bidirectional buck/boost DC-DC converter, are given in following subsections. and also to regulate the speed for achieving MPPT from the wind turbine. The field oriented vector control (FOVC) is used for RSC to generate the switching pulses, as shown in Fig. 2. In FOVC, direct axis and quadrature axis components of rotor currents (I * dr, I * qr) represent reactive and active components, respectively.

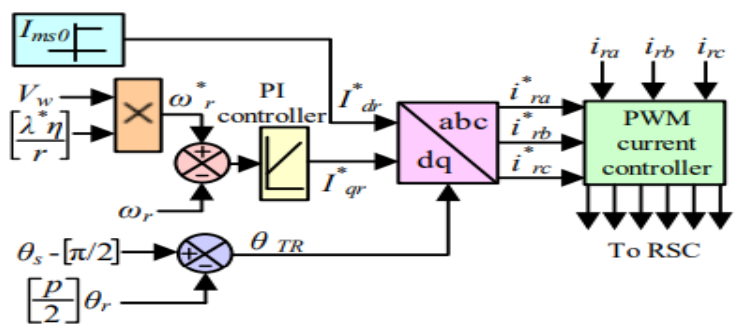

Fig. 3.1. RSC control algorithm.

The I * dr is corresponding to no load magnetizing current (Ims0) of DFIG, which is computed as

$$I_{ms0} = \frac{\sqrt{2}V_L}{\sqrt{3}X_m} \qquad (1)$$

where Xm denotes the magnetizing reactance of the machine and VL is the line voltage at the machine terminals. The I * qr is estimated by passing the speed error through proportional and integral (PI) controller as depicted in Fig. 2 and it is derived as,

$$I^*_{qr(k)} = I^*_{qr(k-1)} + K_{p\omega}(\omega_{err(k)} - \omega_{err(k-1)}) + K_{i\omega}\omega_{err(k)} \qquad (2)$$

where Kpω and Kiω represent proportional and integral constants of PI speed controller, respectively. The ωerr(k) and ωerr(k-1) denote speed error at kth and (k-1)th instants, respectively. The ωerr(k), is obtained as,

$$\omega_{err(k)} = \omega^*_{r(k)} - \omega_{r(k)} \qquad (3)$$

where ω* r(k) and ωr(k) denote the reference and sensed rotor speed of DFIG at kth instant, respectively. The reference rotor speed is obtained from the tip speed ratio MPPT control as,

$$\omega^*_r = \eta\lambda^* V_w / r \qquad (4)$$

Index in Cosmos

May 2024, Volume 14, ISSUE 2

UGC Approved Journal

International journal of basic and applied research

www.pragatipublication.com

ISSN 2249-3352 (P) 2278-0505 (E)

Cosmos Impact Factor-5.86

where Vw, λ * , η and r represent wind speed, optimal tip speed ratio, gear ratio and radius of wind turbine, respectively. The rotor transformation angle (θTR) is computed as,

$$\theta_{TR} = \left(\theta_s - \frac{\pi}{2}\right) - \left(\frac{p}{2}\right)\theta_r \qquad (5)$$

where θs is obtained from phase locked loop and θr is computed from the sensed rotor speed as,

$$\theta_r = \int_0^t (\omega_r)dt \qquad (6)$$

Finally, reference rotor currents (i * ra, i * rb and i * rc) are derived from I * qr and I * dr using an angle of transformation θTR, as depicted in Fig. 2. These reference currents along with sensed rotor currents (ira, irb and irc), are applied to pulse width modulation (PWM) controller to produce RSC gating signals.

B. Control Algorithm for LSC

The LSC control algorithm is depicted in Fig. 3. The LSCis controlled to achieve the following objectives.

- It maintains the DG and DFIG stator currents sinusoidal and balanced.

- It regulates the DG power within the range of PDmin to PDmax to achieve optimal fuel consumption. Where PDmin and PDmax refer to minimum and maximum DG power output in pu for optimal fuel consumption.

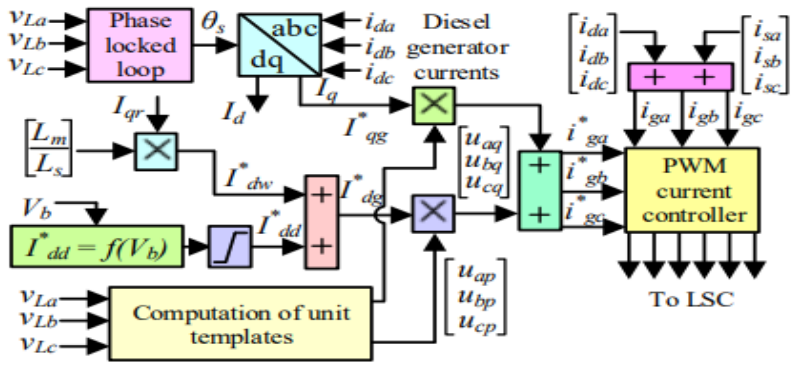

Fig. 3.2 LSC control algorithm.

A modified indirect vector control based on voltage oriented reference frame, is used to generate the reference currents as shown in Fig. 3. In this, both DG and DFIG stator currents are added and controlled to extract maximum power from the DFIG and to regulate the DG power within the range for optimal fuel consumption. The d-axis component of LSC is obtained as,

$$I^*_{dg} = I^*_{dd} + I^*_{dw} \qquad (7)$$

where I * dd, I * dw denote the d-component current of DG and DFIG, respectively. It is noted that the saturation block is placed before the I * dd component to operate the DG in optimal fuel efficient zone at change in load, as depicted in Fig. 3. In this work, a generalized concept is used to calculate the DG power based on state of the BES. The reference DG power in pu (P * D) is computed as,

$$P^*_D = P_{D\min} + k_1\beta \qquad (8)$$

Here the value of β varies from 0 to 1. The minimum value of β is achieved when BES is charged to maximum voltage (Vbmax) whereas β takes maximum value when BES voltage falls to its minimum value (Vbmin). The β is of the form as,

$$\beta = \frac{V_{b\max} - V_b}{k_2} \qquad (9)$$

In (8) and (9), k1 and k2 represent constant parameters. The value of k1 is selected such that P * D attains its maximum limit of optimal fuel consumption as β tends to unity. Moreover, the value of k2 is selected such that the β attains unity at Vbmin. In this work, the chosen values of PDmin, PDmax, Vbmax, Vbmin, k1 and k2 are mentioned in Appendices. From (8), the I * dd is computed as,

$$I^*_{dd} = \left(\sqrt{2/3}\right) \times \left(\frac{P^*_D \times VA_{DG}}{V_L}\right) \qquad (10)$$

where VL and VADG represent line voltage at PCC and VA rating of DG, which is chosen as a base value. The I * dw is computed as,

$$I^*_{dw} = \left(\frac{L_m}{L_s}\right) I_{qr} \qquad (11)$$

The DG currents (ida, idb and idc) are transformed to Id and Iq using angle of transformation (θs), which is obtained from PLL as shown in Fig. 3. The q-axis component of LSC current (I * qg) is numerically same as Iq of DG. The I * dg and I * qg are multiplied with in-phase and quadrature unit templates, respectively and then added together to generate current references (i * ga, i * gb and i * gc). The unit templates are obtained from phase voltages (va, vb and vc), as shown in Fig. 3. Unit templates of in-phase components are obtained as,

$$u_{ap} = \frac{v_a}{V_m}, u_{bp} = \frac{v_b}{V_m}, u_{cp} = \frac{v_c}{V_m} \qquad (12)$$

where, Vm denotes the peak of phase voltage at PCC, which is computed as

$$V_m = \left\{2\left(v_a^2 + v_b^2 + v_c^2\right)/3\right\}^{1/2} \qquad (13)$$

The unit templates of quadrature components, are obtained from in-phase components as

$$u_{aq} = -\frac{u_{bp}}{\sqrt{3}} + \frac{u_{cp}}{\sqrt{3}}, u_{bq} = \frac{\sqrt{3}u_{ap}}{2} + \frac{u_{bp} - u_{cp}}{2\sqrt{3}}, \quad u_{cq} = -\frac{\sqrt{3}u_{ap}}{2} + \frac{u_{bp} - u_{cp}}{2\sqrt{3}} \qquad (14)$$

Finally, the generated reference currents and sensed currents (iga, igb and igc) are applied to PWM controller to produce pulses for LSC, as depicted in Fig. 3.

C. Solar PV Array MPPT Algorithm and Bidirectional Buck/Boost DC-DC Converter Control

The bidirectional buck or bidirectional boost DC-DC converter is used to regulate the DC link voltage by controlling power flow through the BES. By doing so, the solar MPPT is achieved. In this, a modified perturb and observe (P&O) algorithm is used, which consists of sampling pulse generation (X) and subsequently estimation of reference DC link voltage (V * dc) as depicted in Figs. 4-5, respectively. Fig. 4 illustrates various steps involved in the generation of sampling pulse 'X'. Here, the sampling pulse is a namegiven to variable 'X'. It varies between digital bits 0 and 1. In Fig. 4, the first step is to get the information of DC link voltage or solar PV voltage (Vdc) and solar PV current (Ipv) at kth instant and computation of instantaneous solar power. The second step is the determination of running average solar power (Psol), which performs the same function as filtering. In case the absolute difference between the running averaged power (Psol) and previously sampled power (P'sol) is less

International journal of basic and applied research

www.pragatipublication.com

ISSN 2249-3352 (P) 2278-0505 (E)

Cosmos Impact Factor-5.86

than 20 W combined with minimum time delay of 0.25 s from previous sampling, the control senses that steady state has arrived. On sensing the steady state, the output of the sampling pulse 'X' becomes '1'. The sampling pulse decides the instant of incremental change in reference DC link voltage (V * dc) or solar PV MPPT voltage. The value of V * dc is updated only if sampling pulse becomes '1'. This is clearly evident from Fig. 5 that depicts the modified P&O MPPT algorithm. Once X becomes '1', the MPPT algorithm checks for Psol(k) > Psol(k-1). If it is yes, then it again checks for Vdc(k) > Vdc(k-1). If it is also yes, then, the new reference DC link voltage becomes V * dc = Vdc(k)+ ΔVdc. Where ΔVdc denotes the small incremental change in DC link voltage. The other scenarios are evident from the Fig. 5. The bidirectional buck/boost DC-DC converter control, is demonstrated in Fig. 6. The outer proportional-integral (PI) controller of the bidirectional buck or bidirectional DC-DC boost converter control, is used to regulate the DC link voltage. Moreover, the output of the outer PI controller is reference battery current (I * b), as depicted in Fig. 6. The inner PI controller is used to track the reference battery current. Moreover, the output of the inner PI controller is the duty ratio (R) of the bidirectional buck/boost DC-DC converter.

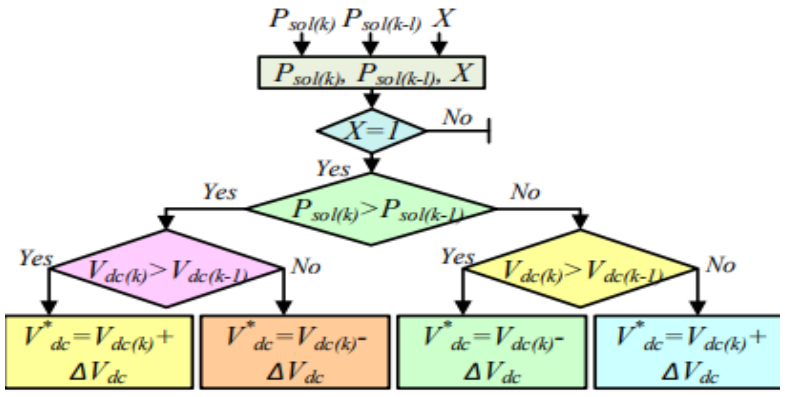

Fig. 3.3. MPPT algorithm of solar PV array.

From Fig. 4, the reference battery current (I * b) is obtained as,

$$I^*_{b(k)} = I^*_{b(k-1)} + K_{pb}(V_{de(k)} - V_{de(k-1)}) + K_{ib}V_{de(k)} \qquad (15)$$

Where, error of the DC link voltage at kth instant is * V V V de k dc k dc k ( ) ( ) ( ) = – . Here V * dc(k) and Vdc(k) represent the reference DC link voltage and sensed DC link bgu -0voltage at kth instant, respectively. Kpb and Kib denote the proportional andintegral constants of the outer PI controller. Besides, the duty ratio (R) of the bidirectional DC-DC converter, is computed as,

$$R_{(k)} = R_{(k-1)} + K_{pr}(I_{be(k)} - I_{be(k-1)}) + K_{ir}I_{be(k)} \qquad (16)$$

Where, error of the battery current at kth instant is * be k b k b k ( ) ( ) ( ) I I I = – . Here I * b(k) and Ib(k) represent the reference battery current and sensed battery current at kth instant, respectively. The obtained duty ratio (R) is applied to PWM generator to produce pulses for the switches of the bidirectional buck or bidirectional boost converter

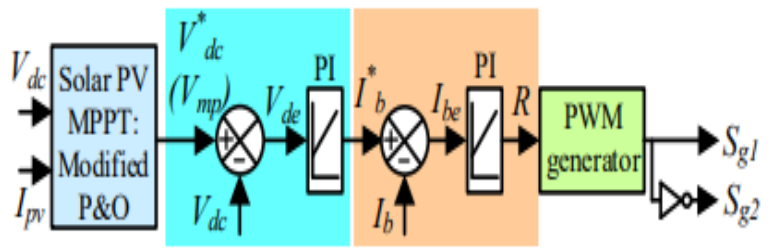

Fig. 3.4. Control of bidirectional buck or bidirectional boost converter.

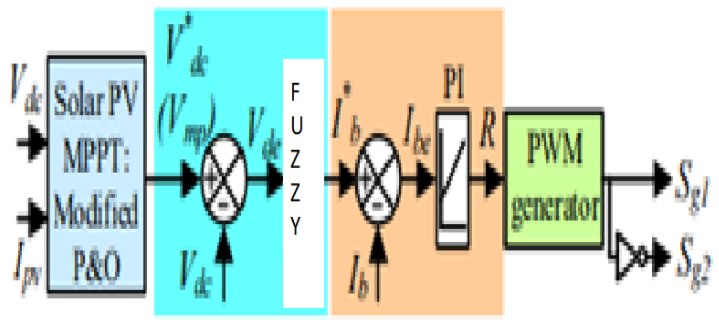

Fig. 3.5. Control of bidirectional buck or bidirectional boost converter, With fuzzy controlled voltage loop

6. SIMULATION DIAGRAM

6.1 SIMULINK CIRCUIT

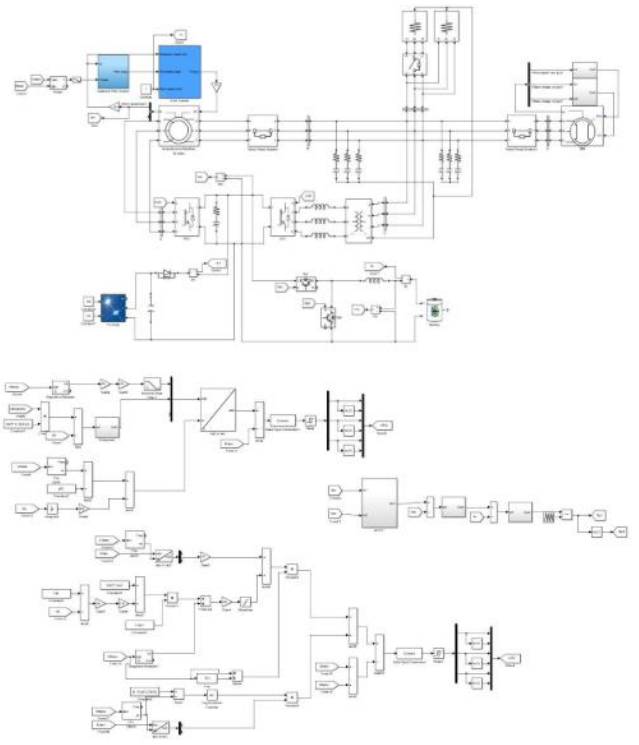

6.2 SIMULATION RESULTS

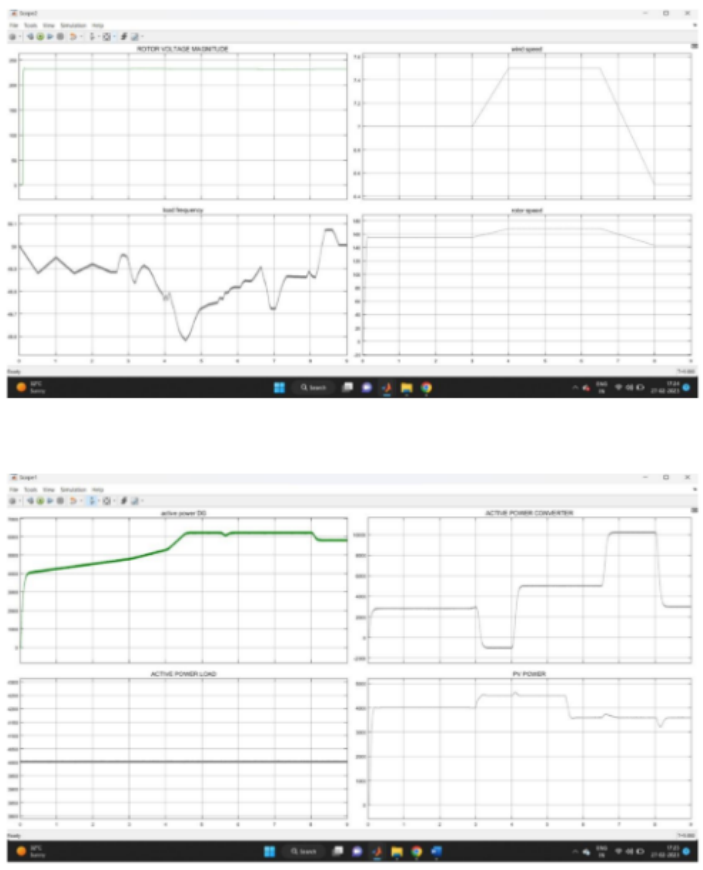

CASE 2

International journal of basic and applied research

www.pragatipublication.com

ISSN 2249-3352 (P) 2278-0505 (E)

Cosmos Impact Factor-5.86

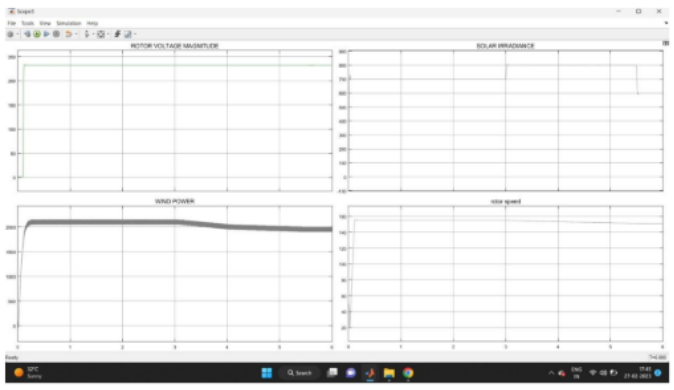

CASE 3

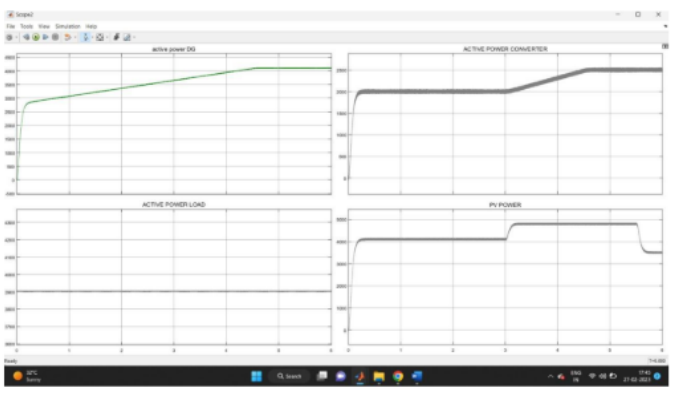

The microgrid based on wind turbine driven DFIG, DG and solar PV array with BES, is simulated using MATLAB. Various signals used to analyze the system performance, are rms value of phase voltage (Vr), system frequency (fL), DFIG rotor speed (ωr), DG power (PD),

wind power from stator (Pw), solar PV power (Psol), load power (PL), LSC power (PLSC), DC link voltage (Vdc), battery current (Ib), battery voltage (Vb), wind speed (Vw), insolation (G), rotor power coefficient (Cp), a-phase stator current (isa), rotor currents (irabc), a-phase DG current (ida), a-phase PCC voltage (vLa), stator currents (isabc), DG currents (idabc), load currents (iLa, iLb and iLc), neutral current (iLn) and LSC currents (icabc).

The parameters used for the simulation are mentioned in Appendices. A. Performance of Bidirectional Buck/Boost DC-DC Converter at Change in Load The performance of bidirectional buck or bidirectional boost DC-DC converter at change in the load, is depicted in Figs. 7 (a-b). The wind speed and insolation are kept at 7 m/s and 700 W/m2 , respectively. Initially a 3-phase balanced load of 2.5 kW is connected at PCC. The DG is delivering 4.84 kW (shown in Fig. 7 (b)), which corresponds to the battery bank voltage of 125 V. Moreover, the DFIG and solar PV array powers are 2.013 kW and 4.122 kW, respectively as depicted in Fig. 7 (b). Since the total generation is more than the localdemand, the remaining power goes to BES through a bidirectional buck/boost DC-DC converter (a). At t = 3 s, an additional load of 2 kW is connected and again it is disconnected at t = 5.5 s. During this period, it is observed that the power generation from all sources, remains unchanged and the increased load power is met by the BES through LSC. There is a minor sag and swell of DC link voltage, however, the solar MPPT is unaffected as seen from Psol waveform. Moreover, the system voltage and frequency are maintained constant,

B. System Performance at Variable Wind Speeds The performance of the system at variable wind speeds are depicted in Figs. 8 (a-c). In this, a 3-phase load of 4 kW is connected at PCC and the insolation is kept at 700 W/m2 . The DG delivers power of 5.67 kW based on the state of the BES, as depicted in Fig. 8 (b). The pattern of wind speed variation is depicted in Fig. 8 (a). It is observed that the controller regulates the DFIG rotor speed as per wind MPPT algorithm, as depicted in Fig. 8 (a). Moreover, it is observed that the DC link voltage is regulated. The system dynamic response during the transition of DFIG speed from supersynchronous to subsynchronous speed region, It is observed that wind MPPT is obtained during the variation of wind speed. Moreover, the frequency rotor currents, is changed according to the speed of operation of DFIG.

C. System Performance at Variable Insolation The performance of the system at varying solar radiation, is depicted in Figs. 9 (a-b). In this, the wind speed is kept constant at 7 m/s. Moreover, the DG delivers 4.2 kW power based on the battery voltage, as depicted in Fig. 9 (b).

In this, a 3-phase linear balanced load of nearly 4 kW is connected at PCC. The insolation of solar PV array is varied from 700 W/m2 to 800 W/m2 at t = 3 s and again it is reduced to 600 W/m2 at t = 5.5 s, as depicted in Fig. 9 (a). The DC link voltage is regulated by the bidirectional DCDC converter control for achieving the solar MPPT. Moreover, the solar MPPT is manifested by the Psol waveform, as depicted in Fig. 9 (a).

D. System Performance at Unbalanced Nonlinear Load The dynamic performance of the system at unbalanced nonlinear load, is depicted in Fig. 10. Initially, a balanced load of 6.7 kW is connected at PCC. It includes a linear load of 0.5 kW and remaining be the nonlinear load, connected on each phase. At t = 2.6 s, a-phase of the load is disconnected and subsequently phase-b, is also disconnected at t = 2.8 s, as depicted in Fig. 10. However, both voltages and currents of DFIG and DG, are maintained balanced and follow the IEEE 519 standard. The LSC helps in unbalance and harmonics compensation of the connected load at PCC. The LSC currents and neutral current, are also shown in Fig. 10. Moreover, the variation of power at unbalanced nonlinear load, is depicted in Fig. 11. Fig. 11 demonstrates waveforms of Vr, Vdc, Ib, Psol, Pw, PD, PL and PLSC. From these results, it is observed that the DC link voltage is regulated and moreover, solar PV and wind MPPT operation is unaffected. The decrease in load power goes to BES through LSC, which is evident from Ib, PL and PLSC waveforms. Moreover, Vr is maintained at constant value.

7. CONCLUSION AND REFERENCES

The microgrid based on wind turbine driven DFIG, DG and solar PV array with BES, with minimum number of converters, has been presented. The solar PV array is directly connected to DC link of back-back connected VSCs, whereas BES is connected through a bidirectional buck/boost DC-DC converter. The system has been simulated for various scenarios such as variable wind speeds, variable insolation and unbalanced nonlinear load connected at PCC. Moreover, the performance of bidirectional buck/boost DC-DC converter at change in the load has been investigated. Simulated results have shown the satisfactory performance of the system to achieve optimal fuel consumption. The DFIG stator voltages, currents and DG currents, are found balanced and sinusoidal, as per the IEEE 519 standard. A prototype has been developed in the laboratory to validate the steady state and dynamic performances of the microgrid. Test results have shown quite good performance under variable wind speeds, linear and nonlinear unbalanced loads and at variable PV insolation.

8.REFERENCES

1. Sambasivaiah Puchalapalli, Member, IEEE, S.K. Tiwari, Bhim Singh, Fellow, IEEE, and P.K. Goel “A Microgrid Based on Wind Driven DFIG, DG and Solar PV Array for Optimal Fuel Consumption”DOI 10.1109/TIA.2020.2999563, IEEE Transactions on Industry Applications, June 17,2020

2. J. Knudsen, J. D. Bendtsen, P. Andersen, K. K. Madsen, and C. H.

3. Sterregaard, “Supervisory control implementation on diesel-driven generator sets,” IEEE Trans. Ind. Electron., vol. 65, no. 12, pp. 96989705, Dec. 2018.

4. J. Jo, H. An, and H. Cha, “Stability improvement of current control by voltage feedforward considering a large synchronous inductance of a diesel generator,” IEEE Trans. Ind. Applicat., vol. 54, no. 5, pp. 51345142, Sept.-Oct. 2018.

5. Y. Zhang, A. M. Melin, S. M. Djouadi, M. M. Olama and K. Tomsovic, “Provision for guaranteed inertial response in diesel-wind systems via model reference control,” IEEE Trans. Power Systems, vol. 33, no. 6, pp. 6557-6568, Nov. 2018.

International journal of basic and applied research

www.pragatipublication.com

ISSN 2249-3352 (P) 2278-0505 (E)

Cosmos Impact Factor-5.86

6. N. Nguyen-Hong, H. Nguyen-Duc, and Y. Nakanishi, “Optimal sizing of energy storage devices in isolated wind-diesel systems considering load growth uncertainty,” IEEE Trans. Ind. Applicat., vol. 54, no. 3, pp. 1983-1991, May-June 2018.

7. W. Li, P. Chao, X. Liang, J. Ma, D. Xu, and X. Jin, “A practical equivalent method for DFIG wind farms,” IEEE Trans. Sustain. Energy, vol. 9, no. 2, pp. 610-620, April 2018.

8. T. Adefarati, R. C. Bansal, and J. John Justo, “Techno-economic analysis of a PV– wind–battery–diesel standalone power system in a remote area,” The Journal of Engineering, vol. 2017, no. 13, pp. 740744, 2017.

9. C. Wu and H. Nian, “Stator harmonic currents suppression for DFIG based on feedforward regulator under distorted grid voltage,” IEEE Trans. Power Electron., vol. 33, no. 2, pp. 1211-1224, Feb. 2018.

10. N. K. Swami Naidu and B. Singh, “Experimental implementation of doubly fed induction generator-based standalone wind energy conversion system,” IEEE Trans. Ind. Applicat., vol. 52, no. 4, pp. 33323339, July-Aug. 2016.

11. D. Sun, X. Wang, H. Nian, and Z. Q. Zhu, “A sliding-mode direct power control strategy for DFIG under both balanced and unbalanced grid conditions using extended active power,” IEEE Trans. Power Electron., vol. 33, no. 2, pp. 1313-1322, Feb. 2018.

12. Ju Liu, Wei Yao, Jinyu Wen, Jiakun Fang, Lin Jiang, Haibo He, and Shijie Cheng,